JOURNAL OF THERMOPHYSICS AND HEAT TRANSFER
Vol. 15, No. 3, July–September 2001

Composite Lumped Model and Algebraic Solutions of Unsteady Temperatures and Accumulated Heat Transfer

Antonio Campo*
Idaho State University, Pocatello, Idaho 83209

Calculations of temperature histories and accumulated heat transfer in simple bodies (long plates, long cylinders, and spheres) for applications in thermal engineering have been traditionally obtained from the standard Heisler/Gröber charts (Heisler, M. P., "Temperature Charts for Induction and Constant Temperature Heating," *Transactions of the American Society of Mechanical Engineers*, Vol. 69, 1947, pp. 227–236 and Gröber, H., *Einführung in die Lehre von der Wärmeübertragung*, Springer, Berlin, 1926). The deterrent of this tandem of charts is that they are exclusively applicable to dimensionless times τ greater than 0.2. From a mathematical perspective, this imposing restriction is associated with the utilization of truncated one-term series for the construction of these charts. For practical purposes, the pair of Heisler charts for each of the three simple bodies is difficult to read, necessitating skillful visual interpolation. The time variations of mean and surface temperatures, as well as the total heat transfer of the three basic bodies via a composite lumped model, are predicted. Then the time variations of the center temperatures in the three bodies are determined from a variant of the integral balance method. This unique alliance turns out to be very accessible and leads to a handful of easily evaluated algebraic expressions at any time, even at arduous dimensionless times less than 0.2, where the standard Heisler/Gröber charts falter.

Nomenclature

A = surface area of body
Bi = Biot number, $\bar{h}_f R/k_s$
c = geometric parameter: 1 for long plate, 2 for long cylinder, and 3 for sphere
c_s = specific heat capacity of solid
$\bar{h}_f$ = mean external convective coefficient
h_s = local internal convective coefficient
$\bar{h}_s$ = mean internal convective coefficient
k = thermal conductivity
m = mass of body
$\overline{Nu}_f$ = mean external Nusselt number, $\bar{h}_f(2R)/k_f$
$\overline{Nu}_{ov}$ = mean overall Nusselt number, $\bar{U}(2R)/k_s$
$\overline{Nu}_s$ = mean internal Nusselt number, $\bar{h}_s(2R)/k_s$
Q_i = initial heat stored
Q_t = total heat transfer
q_w = surface heat flux
R = semithickness of long plate, radius of long cylinder, and radius of sphere
r = transverse coordinate
r^* = transverse coordinate for the semi-infinite region
T = temperature
T_c = center temperature
T_i = initial temperature
T_m = mean temperature
T_w = surface temperature
T_∞ = temperature of fluid
t = time
U = local overall heat transfer coefficient
$\bar{U}$ = mean overall heat transfer coefficient
V = volume of body
α_s = thermal diffusivity of solid, $k_s/\rho_s c_s$
η = dimensionless r
η^* = dimensionless r for the semi-infinite region
θ = dimensionless T for convective surface
ρ = density
τ = dimensionless t or Fourier number, $t/(L^2/\alpha_s)$
ψ = dimensionless T for isothermal surface
Ω_t = dimensionless Q_t

Subscripts

f = fluid
s = solid

Received 18 October 1999; revision received 4 October 2000; accepted for publication 5 October 2000.

*Professor, College of Engineering. Member AIAA.

Introduction

AMONG the repertoire of methods available for solving parabolic partial differential equations, the method of separation of variables is unequivocally the most popular for the solution of unsteady heat conduction in regular bodies (long plate, long cylinder, and sphere) exposed to a convective environment (see Arpaci[1]). This technique leads to infinite Fourier and Bessel–Fourier series for the prediction of the unsteady temperatures and accompanying total heat transfer in the three regular bodies. Invariably, for purposes of numerical evaluation of local temperatures, mean temperatures, and total heat transfer, the pressing characteristic of these infinite series is that they converge rapidly for long times necessitating only one term. However, the infinite series diverges dramatically for short times, even violating the imposed initial condition in some instances. As a result of this ambiguity, numerous terms must be retained in the infinite series to secure good convergence for short times. For practical applications of thermal engineering, the resultant infinite series have been traditionally truncated to one term generating the one-term series, also called the long-time solutions. In this regard, Grigull et al.[2,3] rigorously investigated the region of validity of the approximate one-term series, when compared with the exact infinite series for the three basic geometries. These authors arrived at the conclusion that the inherent errors are within 1% when the dimensionless times τ exceeded 0.18 for the long plate, 0.21 for the long cylinder, and 0.24 for the sphere, respectively. For conciseness, analysts have conveniently encapsulated these three cutoff numbers into an approximate mean value of 0.2.

From a chronological standpoint, Gurney and Lurie,[4] inspired by the simplistic one-term series valid for $\tau \geq 0.2$, created the first temperature–time charts as early as 1923. In 1945, Boelter et al.[5] framed the second temperature–time diagrams without using the restrictive one-term series, so that their diagrams are valid at any time. The one-term series approach was exploited again by Heisler[6] in 1947 for the construction of a pair of temperature–time charts

for the center and surface of each body suitable for $\tau \geq 0.2$. He also provided refined short-time charts for $\tau < 0.2$ with reasonable truncations of the infinite series. Despite that, the Heisler short-time charts are infrequently mentioned in the heat exchange literature; they may be found in the book by Gebhart.[7]

Experience ratifies that the reading of center temperatures in the first Heisler charts (parameterized by the Biot number) is a demanding task. In most practical applications in thermal engineering, the Biot number is not precisely an integer number, and the reading in the first Heisler charts becomes difficult necessitating skillful visual interpolation. Also, ingenious visual interpolation is indispensable for the reading of the logarithmic ordinates in the first Heisler charts. Another anomaly of the first Heisler charts is that they cannot be read precisely because the straight lines are clustered in the upper left corners. In addition, the intervals in the abscissas of the charts were nonuniformly spaced. Fortunately, when the second Heisler charts (parameterized by the dimensionless space variable) are used, reading of temperatures at other locations off the center is not that difficult except that the lines are agglomerated in the upper right corners. Needless to say, an erroneous reading in the first Heisler charts may propagate into the second Heisler charts distorting the magnitude of offcenter temperatures. The errors show a magnifying pattern as the location moves outward from the center toward the surface; the largest errors occur at the surface temperatures. The surface temperatures are essential for the estimation of convection heat transfer coefficients in the platform of inverse heat conduction problems. Furthermore, calculations of the accumulated heat transfer were normally done with the Gröber charts (see Gröber[8] and Gröber et al.[9]), which again are sound for $\tau \geq 0.2$.

An important question pertaining to the standard Heisler charts that needs to be raised is the following: What are the options that analysts have when they are faced with the task of calculating unsteady temperatures in regular bodies whenever the Fourier numbers τ are less than 0.2? For these short times, the best possible way for addressing this issue is by evaluating a dependable number of eigenvalues appropriate to the infinite series for the body in question. Stevens and Luck[10] have recently reported compact expressions for the prediction of this collection of eigenvalues in terms of the Biot number for long plates, long cylinders, and spheres. Adebiyi[11] used a geometric parameter ω (0 for the long plate, 1 for the long cylinder, and 2 for the sphere) and wrote the heat conduction equation for each shape as a single generalized heat conduction equation. The associated Sturm–Liouville problem resulted in a Bessel equation, so that the temperature solutions were expressed by Bessel functions of three different orders. Another plausible option is to solve the unidirectional heat equation in rectangular, cylindrical, and spherical coordinate systems with the explicit formulation of finite differences (see Ribando and O'Leary[12]). In addition, some textbooks on heat conduction[1] insinuate the use of temperature–time results based on the idealization of a semi-infinite region. In reference to this region, the temperature–time plots for a prescribed surface temperature ($Bi \to \infty$) drawn by Luikov[13] reveals that the Fourier numbers have to be within 0.05 for the long plate, 0.04 for the long cylinder, and 0.03 for the sphere, respectively.

To avoid the utilization of the standard Heisler/Gröber charts[6,8] on the one hand and the evaluation of near infinite Fourier and Bessel–Fourier series on the other hand, this paper develops a composite lumped model that is conjoined with a variant of the integral balance method. The composite lumped model accounts for the two thermal resistances overseeing the problem of unsteady unidirectional heat conduction in simple bodies with symmetric convection cooling. Generally speaking, the easy-to-evaluate algebraic solutions may permit the rapid determination of the spatio–temporal variation of the relevant local temperatures (center and surface), the global mean temperatures, and the total heat transfer rates for the entire time domains, including the subdomain $\tau < 0.2$. These algebraic calculations can be done efficiently with a hand calculator.

Composite Lumped Model

Consider the unsteady and unidirectional conduction of heat in a solid regular body (long plate, long cylinder, and sphere) possessing uniform temperature T_i initially. For $t > 0$, the body surface(s) exchange heat by convection with a surrounding fluid, which is characterized by a constant temperature T_∞ and a mean, external convective coefficient $\bar{h}_f$. The thermophysical properties of the material are assumed as independent of temperature. The three solid bodies under study and the corresponding coordinate systems are shown in Fig. 1.

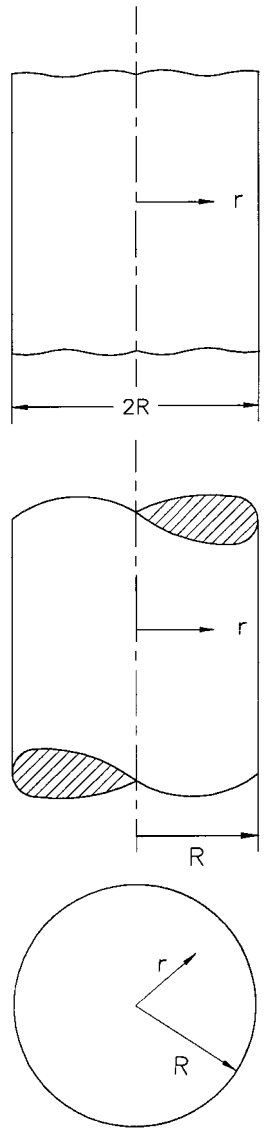

Fig. 1 Simple bodies and their corresponding coordinate systems.

Mean and Surface Temperature Distributions

A thermodynamic control volume is described by a differential element of thickness Δt inside a regular body with a uniform surface temperature T_w. Performing a lumped-based energy balance on the control volume supplies the lumped equation

$$\rho_s c_s V \frac{\mathrm{d}T_m}{\mathrm{d}t} = -U A (T_m - T_\infty), \qquad T_m(0) = T_i \tag{1}$$

In this ordinary differential equation of first order, the two dominant variables are the mean temperature T_m, defined by

$$T_m(t) = \frac{1}{V} \int_V T(\boldsymbol{x}, t)\, \mathrm{d}V \tag{2}$$

and the local, overall heat transfer coefficient U (Ref. 1). Conceptually, U links the conduction of heat inside the solid body and the convection of heat between the body surface and the fluid. Therefore, U is affected by the local internal and external convective

coefficient h_s and the mean external convective coefficient $\bar{h}_f$ in the following way:

$$U = 1/(1/h_s + 1/\bar{h}_f) \tag{3}$$

This formula has statistical significance because it establishes a harmonic mean of h_s and $\bar{h}_f$ at each time t.

After separating variables in Eq. (1), this equation may be rewritten as follows:

$$\rho_s c_s V \frac{\mathrm{d}T_m}{(T_m - T_\infty)} = -U(t) A \, \mathrm{d}t \tag{4}$$

First, multiplying the right-hand side of Eq. (4) by t/t and, later, integrating the entire equation between the suitable limits for the dependent variable T_m and the independent variable t yield

$$\rho_s c_s V \int_{T_i}^{T_m} \frac{\mathrm{d}T_m}{(T_m - T_\infty)} = -At\left[\frac{1}{t}\int_0^t U(t)\,\mathrm{d}t\right] \tag{5}$$

It is easy to recognize on the right-hand side of the preceding equation that the expression inside the brackets is the mean, overall heat transfer coefficient whose definition is

$$\bar{U}(t) = \frac{1}{t}\int_0^t U(t)\,\mathrm{d}t \tag{6}$$

Next, integrating the left-hand side of Eq. (5) and rearranging terms delivers the single-term mean temperature distribution

$$T_m = T_\infty + (T_i - T_\infty)\exp\left(-\frac{A\bar{U}(t)}{\rho_s c_s V}t\right) \tag{7}$$

where the numerical value of $\bar{U}$ is taken from the relation

$$\bar{U} = 1/(1/\bar{h}_s + 1/\bar{h}_f) \tag{8}$$

Furthermore, introducing the customary dimensionless variables θ for temperature and τ for time, along with the dimensionless group $\overline{Nu}_{\mathrm{ov}}$ called the mean, overall Nusselt number

$$\theta = \frac{T - T_\infty}{T_i - T_\infty}, \qquad \tau = \frac{t}{R^2/\alpha_s}, \qquad \overline{Nu}_{\mathrm{ov}} = \frac{\bar{U}(2R)}{k_s} \tag{9}$$

enables us to transform Eq. (8) into an equivalent relation,

$$\overline{Nu}_{\mathrm{ov}} = 1/[1/\overline{Nu}_s + 1/(k_f/k_s)\overline{Nu}_f] \tag{10}$$

where $\overline{Nu}_{\mathrm{ov}}$ controls the combined heat exchange at a specific time. Note that $\overline{Nu}_{\mathrm{ov}}$ constitutes a weighted harmonic mean of the mean, internal Nusselt number $\overline{Nu}_s$ and the mean, external Nusselt number $\overline{Nu}_f$. The prevalent weight of $\overline{Nu}_f$ is the thermal conductivity ratio between the external fluid and the solid, that is, k_f/k_s.

In the analysis of unsteady conduction of heat, the dimensionless version of the mean external convective coefficient $\bar{h}_f$ is normally given by the Biot number Bi and not by the mean external Nusselt number $\overline{Nu}_f$. The bottom line here is that both numbers may be used on realizing that Bi and $\overline{Nu}_f$ are interrelated by

$$Bi = \tfrac{1}{2}(k_f/k_s)\overline{Nu}_f \tag{11}$$

Hence, the proportionality constant is the thermal conductivity ratio between the external fluid and the solid, that is, k_f/k_s, namely, the weight in Eq. (10). Accordingly, the combination of Eqs. (10) and (11) leads to the alternate form

$$\overline{Nu}_{\mathrm{ov}} = 1/(1/\overline{Nu}_s + 1/2Bi) \tag{12}$$

In addition, the dimensionless representation of the mean temperature distribution [Eq. (7)] turns out to be

$$\theta_m = \exp[-(c/2)\overline{Nu}_{\mathrm{ov}}\tau] \tag{13}$$

which essentially is valid at any dimensionless time τ without restriction (even for $\tau < 0.2$). The geometric parameter c appearing in Eq. (13) assumes values of 1 for a long plate, 2 for a long cylinder, and 3 for a sphere. In retrospect, Eq. (13) may be interpreted as the analytic solution of the correspondent lumped equation

$$\frac{\mathrm{d}\theta_m}{\mathrm{d}\tau} = -\frac{c}{2}\overline{Nu}_{\mathrm{ov}}\,\theta_m, \qquad \theta_m(0) = 1 \tag{14}$$

The second temperature of importance in unsteady heat conduction is the surface temperature of the body, θ_w. This local temperature may be easily extracted from a suitable combination of two of the thermal resistances that govern the problem. For instance, one possible choice is to employ the ratio

$$\theta_w = \theta_m[1 - (\overline{Nu}_{\mathrm{ov}}/\overline{Nu}_s)] \tag{15}$$

Center Temperature Distributions

The third temperature of (lesser) importance in unsteady heat conduction is the center temperature of the body, θ_c. Fundamentally, this local interior temperature cannot be obtained from a lumped model. However, an elementary procedure inspired by the integral balance method of Goodman,[14] has been implemented in this subsection for the prediction of θ_c. Accordingly, let us propose a trial temperature profile in the form of a power series:

$$\theta(\eta) = a_0 + a_1(1 - \eta) + a_2(1 - \eta^2) + \cdots + a_n(1 - \eta^n) \tag{16}$$

where the constants a are attached to a specific dimensionless time τ. The assumed temperature profile must satisfy the boundary conditions associated with the formal differential model, together with other required physical conditions.[14] Actually, we can identify a total of four conditions: 1) the dimensionless temperature at the surface is $\theta(1) = \theta_w$, 2) the dimensionless temperature gradient at the center is $\mathrm{d}\theta(0)/\mathrm{d}\eta = 0$, 3) a local energy balance at the surface stipulates that $-\mathrm{d}\theta(1)/\mathrm{d}\eta = Bi\theta_w$, and 4) the dimensionless mean temperature θ_m must satisfy the relation

$$\theta_m = c\int_0^1 \theta\eta^{c-1}\,\mathrm{d}\eta = f(a_2, a_3) \tag{17}$$

Once conditions 1 and 2 have been fulfilled, the trial temperature profile of Eq. (16) evolves into a curtailed cubic polynomial

$$\theta(\eta) = \theta_w + a_2(1 - \eta^2) + a_3(1 - \eta^3) \tag{18}$$

which is absent the first-order term $a_1(1 - \eta)$. A direct consequence of this finding is that an adjoint system of two algebraic equations in two unknowns (constants a_2 and a_3) needs to be solved. The proper system of equations is composed of condition 3 and the equation

$$Bi\theta_w = 2a_2 + 3a_3 \tag{19}$$

which comes directly from condition 4, that is, Eq. (17), once particularized at the three values of the geometric parameter $c = 1$, 2, and 3. In this type of system, the dimensionless mean temperature θ_m and the dimensionless surface temperature θ_w are quantities known in advance from the utilization of the composite lumped model. Accordingly, the three specific cubic polynomials, capable of describing the temperature profiles for the three geometries, need to be constructed.

Long Plate

Introducing Eq. (18) into Eq. (17) for $c = 1$,

$$\theta_m = \int_0^1 \theta\,\mathrm{d}\eta = f_p(a_2, a_3) \tag{20}$$

gives the dimensionless mean temperature

$$\theta_m = \theta_w + \tfrac{3}{4}a_2 + \tfrac{2}{3}a_3 \tag{21}$$

Solving the system of two equations yields the expressions for a_2 and a_3:

$$a_2 = -4\theta_m + 4\theta_w + \tfrac{4}{3}Bi\theta_w \tag{22}$$

$$a_3 = 6\theta_m - 6\theta_w - \tfrac{3}{2}Bi\theta_w \tag{23}$$

Evaluating Eq. (18) delivers the dimensionless temperature profile, whose value at the centerplane, $\eta = 0$, is

$$\theta_c = 2\theta_m - \theta_w - \tfrac{1}{6}Bi\theta_w \tag{24}$$

Long Cylinder

Introducing Eq. (18) into Eq. (17) for $c = 2$,

$$\theta_m = 2\int_0^1 \theta\eta\,\mathrm{d}\eta = f_c(a_2, a_3) \tag{25}$$

gives the dimensionless mean temperature

$$\theta_m = \theta_w + \tfrac{3}{5}a_2 + \tfrac{1}{2}a_3 \tag{26}$$

Solving the system of equations yields the expressions for a_2 and a_3:

$$a_2 = -\tfrac{20}{3}\theta_m + \tfrac{20}{3}\theta_w + \tfrac{5}{3}Bi\theta_w \tag{27}$$

$$a_3 = 10\theta_m - 10\theta_w - 2Bi\theta_w \tag{28}$$

Evaluating Eq. (18) delivers the dimensionless temperature profile, whose value at the centerline, $\eta = 0$, is

$$\theta_c = \tfrac{10}{3}\theta_m - \tfrac{7}{3}\theta_w - \tfrac{1}{3}Bi\theta_w \tag{29}$$

Sphere

Introducing Eq. (18) into Eq. (17) for $c = 3$,

$$\theta_m = 3\int_0^1 \theta\eta^2\,\mathrm{d}\eta = f_s(a_2, a_3) \tag{30}$$

gives the dimensionless mean temperature

$$\theta_m = \theta_w + \tfrac{1}{2}a_2 + \tfrac{2}{5}a_3 \tag{31}$$

Solving the system of equations yields the expressions for a_2 and a_3:

$$a_2 = -10\theta_m + 10\theta_w + 2Bi\theta_w \tag{32}$$

$$a_3 = 15\theta_m - 15\theta_w - \tfrac{5}{2}Bi\theta_w \tag{33}$$

Evaluating Eq. (18) delivers the dimensionless temperature profile, whose value at the center, $\eta = 0$, is

$$\theta_c = 5\theta_m - 4\theta_w - \tfrac{1}{2}Bi\theta_w \tag{34}$$

Note that another conceivable option for the trial temperature profile could have been

$$\theta(\eta) = b_0 + b_1\eta + b_2\eta^2 + \cdots + b_n\eta^n \tag{35}$$

However, this alternate route turns out to be more elaborate because it necessitates the construction of adjoint systems of three algebraic equations. Instead, simpler systems of two algebraic equations were obtained with the $a_n(1 - \eta^n)$ format of the trial temperature profile of Eq. (16).

Total Heat Transfer

Calculation of the total heat transfer Q_t between the initial time $t = 0$ and a final time level t in the three bodies may be computed directly and rapidly using a global energy balance:

$$Q_t = m_s c_s[T_i - T_m(t)] \tag{36}$$

By virtue of the dimensionless heat transfer (or the heat transfer efficiency), $\Omega_t = Q_t/Q_\infty$, the preceding equation may be rewritten in dimensionless form as

$$\Omega_t = 1 - \theta_m(\tau) \tag{37}$$

Q_∞ is the amount of heat stored initially in a body and is quantified by the limiting relation

$$Q_\infty = m_s c_s(T_i - T_\infty) \tag{38}$$

The equality between the total heat transfer Ω_t and the temperature difference $[1 - \theta_m(\tau)]$ in Eq. (37) establishes a one-to-one correspondence between the two thermal quantities of global character. The thermodynamic procedure of this subsection seeks to supplant the use of the Gröber charts[8] for the calculation of total heat transfer in the three bodies.

Presentation of Results

To assess the accuracy of the algebraic-intensive unsteady temperatures produced by the composite lumped model and the variant of the integral balance method, the three baseline solutions that are accessible to us are 1) the numerical evaluation of the infinite series, where the eigenvalues depend on Bi; 2) the Heisler short-time charts[6] for $\tau < 0.2$; and 3) the Boelter et al. diagrams[5] effective at all times. For purposes of comparison, we opted for the Heisler short-time charts[6] in favor of the Boelter et al. diagrams.[5] The rationale for this choice is that the former are easier to read and, even more important, cover a wider range of Biot number, which goes up to 20.

The first two temperatures that need to be computed via a composite lumped model are the mean temperatures θ_m (global quantity) and the surface temperatures θ_w (local quantity). Later, the center temperatures θ_c (local quantity) are determined by the integral balance method. These three temperatures are obtained for suitable pairs of Biot number and τ. The largest and smallest values of Biot number used in the Heisler short-time charts[6] are 20 and $1/0.6 = 1.667$, respectively. Literally, $Bi = 20$ identifies a vigorous cooling, where the internal conductive resistance dominates the external convective resistance, whereas for moderate cooling it is characterized by comparable resistances inside the body and between the body surface and the fluid, namely, Biot number of order one, for example, $Bi = 1.667$. Besides, the dimensionless times in the abscissa of the Heisler short-time charts ran from 0 to 0.2. Therefore, to carry out the algebraic temperature calculations, it was deemed reasonable to choose three values of $\tau \leq 0.2$, namely, $\tau = 0.2$, 0.1, and 0.05.

The mean internal Nusselt number $\overline{Nu}_s$ for bodies with isothermal surfaces may be determined from three different sources: 1) the infinite series [Eq. (A13)], 2) the transversal method of lines (TMOL) [Eqs. (A21), (A23), (A25) and (A26)], and 3) the semi-infinite region [Eqs. (A26) and (A31)] (see the Appendix).

It is widely known that among the three basic shapes, the long plate, the long cylinder, and the sphere, the spherical configuration exhibits the highest rate of cooling because of its favorable volume/surface area ratio. Because of this individual feature, we have chosen this geometry to conduct the comparison tests.

Although the mean temperatures θ_m are unavailable from the Heisler short-time charts,[6] if necessary, a simple numerical integration with Simpson's rule is always possible. Once θ_m are accurately computed by the composite lumped model, the accumulated or total heat transfer Ω_t can be easily determined with the help of Eq. (37). This single step supersedes the use of the Gröber charts.[8]

An overall inspection of the mean, surface, and center temperatures in the sphere, in conjunction with the temperature deviations listed in Tables 1–6, reveals that the accuracy provided for the estimation of Nusselt number $\overline{Nu}_s$ by the infinite series and the TMOL

Table 1 Comparison of the three relevant temperatures for $Bi = 20$ and $\tau = 0.2$

Parameter	Exact	Infinite series	TMOL	Semi-infinite region
$\overline{Nu}_{s,0}$	——	——	4.937	7.046
$\overline{Nu}_s$	——	8.306	8.226	9.640
$\overline{Nu}_{ov}$	——	6.878	6.823	7.768
θ_m	0.10	0.127	0.129	0.097
		(0.027)[a]	(0.029)	(−0.003)
θ_w	0.025	0.022	0.022	0.019
		(−0.003)	(−0.003)	(−0.006)
θ_c	0.35[b]	0.327	0.337	0.219
		(−0.023)	(−0.013)	(−0.131)

[a]Deviations between approximate and exact temperatures appear between parentheses.
[b]Reading from the Boelter et al. diagram[5] is 0.34.

Table 2 Comparison of the three relevant temperatures for $Bi = 20$ and $\tau = 0.1$

Parameter	Exact	Infinite series	TMOL	Semi-infinite region
$\overline{Nu}_{s,0}$	——	——	7.037	9.136
$\overline{Nu}_s$	——	9.730	9.634	11.259
$\overline{Nu}_{ov}$	——	7.826	7.764	8.786
θ_m	——	0.309	0.312	0.268
θ_w	0.05	0.06	0.061	0.059
		(0.01)[a]	(0.011)	(0.009)
θ_c	0.75[b]	0.705	0.706	0.514
		(−0.045)	(−0.044)	(−0.236)

[a]Deviations between approximate and exact temperatures appear between parentheses.
[b]Reading from the Boelter et al. diagram[5] is 0.73.

Table 3 Comparison of the three relevant temperatures for $Bi = 20$ and $\tau = 0.05$

Parameter	Exact	Infinite series	TMOL	Semi-infinite region
$\overline{Nu}_{s,0}$	——	——	9.814	12.093
$\overline{Nu}_s$	——	12.086	11.816	13.767
$\overline{Nu}_{ov}$	——	9.282	9.122	10.242
θ_m	——	0.499	0.505	0.464
θ_w	0.105	0.116	0.115	0.119
		(0.011)[a]	(0.01)	(0.014)
θ_c	0.965[b]	0.871	0.915	0.654
		(−0.094)	(0.05)	(−0.311)

[a]Deviations between approximate and exact temperatures appear between parentheses.
[b]Reading from the Boelter et al. diagram[5] is 0.92.

Table 4 Comparison of the three relevant temperatures for $Bi = 1.667$ and $\tau = 0.2$

Parameter	Exact	Infinite series	TMOL	Semi-infinite region
$\overline{Nu}_{s,0}$	——	——	4.937	7.046
$\overline{Nu}_s$	——	8.306	8.226	9.640
$\overline{Nu}_{ov}$	——	2.379	2.372	2.477
θ_m	——	0.490	0.491	0.476
θ_w	0.35	0.350	0.349	0.354
		(0.0)[a]	(−0.001)	(0.004)
θ_c	0.68[b]	0.758	0.768	0.669
		(0.078)	(0.088)	(−0.001)

[a]Deviations between approximate and exact temperatures appear between parentheses.
[b]Reading from the Boelter et al. diagram[5] is 0.66.

are of comparable quality. In contrast, the accuracy of the three temperatures suffers a bit when the semi-infinite region is implemented.

Irrespective of the three possible approaches that could be adopted for the estimation of Nusselt number $\overline{Nu}_s$, the largest temperature discrepancy must be expected to occur at the center of the sphere largely because of the inherent deficiency of the integral balance method at this location. In fact, when the infinite series is utilized through Eq. (A13), the θ_c deviations disclose a monotonic growth

Table 5 Comparison of the three relevant temperatures for $Bi = 1.667$ and $\tau = 0.1$

Parameter	Exact	Infinite series	TMOL	Semi-infinite region
$\overline{Nu}_{s,0}$	——	——	7.037	9.136
$\overline{Nu}_s$	——	9.730	9.634	11.259
$\overline{Nu}_{ov}$	——	2.483	2.477	2.572
θ_m	——	0.689	0.690	0.680
θ_w	0.50	0.513	0.513	0.525
		(0.013)[a]	(0.013)	(0.025)
θ_c	0.915[b]	0.965	0.970	0.862
		(0.05)	(0.055)	(−0.053)

[a]Deviations between approximate and exact temperatures appear between parentheses.
[b]Reading from the Boelter et al. diagram[5] is 0.88.

Table 6 Comparison of the three relevant temperatures for $Bi = 1.667$ and $\tau = 0.05$

Parameter	Exact	Infinite series	TMOL	Semi-infinite region
$\overline{Nu}_{s,0}$	——	——	9.814	12.093
$\overline{Nu}_s$	——	12.086	11.816	13.767
$\overline{Nu}_{ov}$	——	2.613	2.600	2.684
θ_m	——	0.822	0.823	0.818
θ_w	0.63	0.644	0.642	0.659
		(0.014)[a]	(0.012)	(0.029)
θ_c	1.00[b]	0.997	1.012	0.905
		(−0.003)	(0.012)	(−0.095)

[a]Deviations between approximate and exact temperatures appear between parentheses.
[b]Reading from the Boelter et al. diagram[5] is 0.97.

with increments in τ for $Bi = 20$, that is, -0.023 at $\tau = 0.2$, -0.045 at $\tau = 0.1$, and -0.094 at $\tau = 0.05$. Also, for $Bi = 1.667$, the θ_c deviations manifest a monotonic decrease with increments in τ, that is, 0.078 at $\tau = 0.2$, 0.05 at $\tau = 0.1$, and 0.003 at $\tau = 0.05$. These numbers clearly reveal that all θ_c deviations lie within a diminutive 0.01 margin in the sensitive subinterval $0.05 < \tau < 0.2$. Certainly, a good agreement for the estimation of the demanding center temperatures is in evidence.

Last, weak cooling implies that the external convective resistance overshadows the internal conductive resistance (small $Bi < 0.1$). This extreme case is governed by a standard lumped model and not by the composite lumped model and, thus, does not need further discussion.

For purposes of visualization, the center and the surface temperatures computed by the composite lumped model and the variant of the integral balance method are marked with black dots in Fig. 2.

Based on the qualitative nature of the temperature comparisons of local and global temperatures in a sphere, it may be inferred without any reservation that the long plate and the long cylinder will exhibit levels of accuracy encompassing smaller θ_c deviations.

Ultimately, the preceding paragraphs outlined compact algebraic expressions for calculating temperature distributions and total heat transfer in one-dimensional bodies exclusively. The product method combines analytic solutions of these one-dimensional bodies via a superposition procedure that generates the analytic solutions of multidimensional bodies in two and three dimensions. Further details and proofs of the applicability of the product method are given by Arpaci.[1] In addition, Langston[15] has demonstrated that the superposition procedure can be equally applied for the estimation of the total heat transfer from multidimensional bodies to neighboring fluids using the total heat transfer as input for the participating unidimensional bodies. This author deduced special algebraic formulas for the group of two- and three-dimensional bodies that are capable of performing this task satisfactorily. Because in the context of the composite lumped model the mean temperature is the principal temperature, the algebraic formulas for the dimensionless total heat transfer in multidimensional bodies developed in Ref. 15 can be simplified significantly in the following manner.

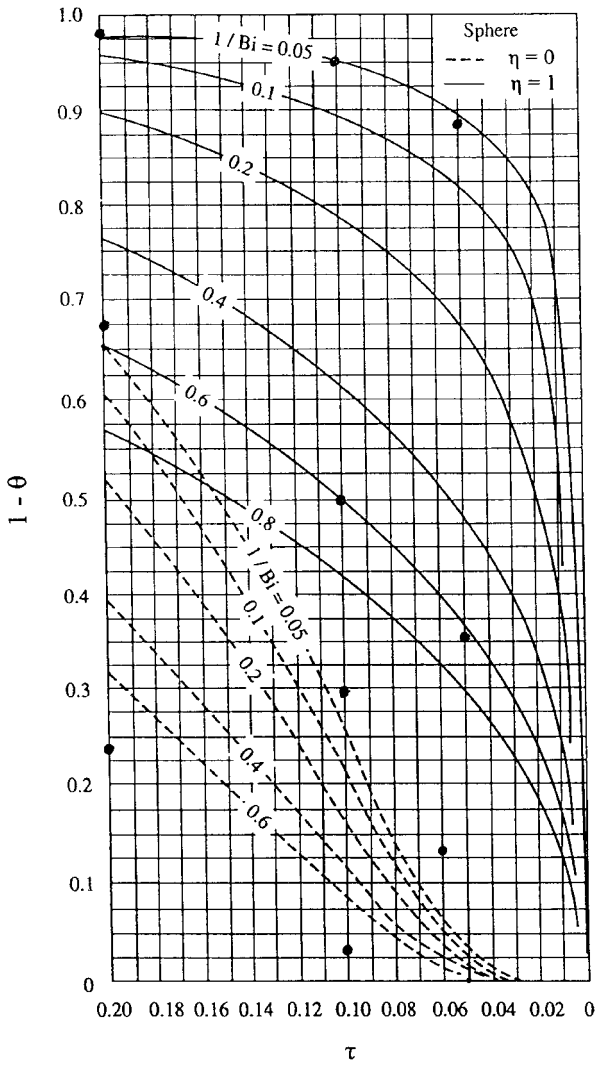

Fig. 2 Comparison of the dimensionless temperatures at the surface and at the center of a sphere as obtained by the composite lumped model and the integral balance method; exact dimensionless temperatures correspond to the Heisler short-time charts.[6]

For a two-dimensional body,

$$\Omega_t = 1 - \theta_{m,1}\theta_{m,2} \tag{39}$$

and for a three-dimensional body,

$$\Omega_t = 1 - \theta_{m,1}\theta_{m,2}\theta_{m,3} \tag{40}$$

In these two compressed equations, the subscripts 1, 2, and 3 identify the participating one-dimensional that form the multidimensional bodies.

Conclusions

It is instinctive to see that the composite lumped model for the analysis of convectively cooled/heated regular bodies consists of two thermal resistances. One is the thermal conductive resistance inside the body, and the other is the thermal convective resistance at the body/fluid interface. The former is quantified by the mean, internal Nusselt number $\overline{Nu}_s$ for isothermal surfaces, whereas the latter is just the Biot number Bi. The Nusselt number $\overline{Nu}_s$ may be computed accurately with the Fourier and Bessel–Fourier infinite series or even with the TMOL.

The intrinsic peculiarity of the composed lumped model is that the mean temperatures, the surface temperatures, and the total heat transfer in regular bodies can be easily evaluated by algebraic means with hand calculators at any dimensionless time τ, without limitation, that is, $0 < \tau < \infty$. The standard Heisler/Gröber charts[6,8] rely on the downgraded one-term series of Fourier and Bessel–Fourier type, and as a result of this, these charts are suited for dimensionless times τ greater than 0.2 exclusively.

The composite lumped model is unqualified to predict the center temperature of bodies simply because this interior temperature cannot be linked to a thermal resistance. A variant of the integral balance method has been devised to estimate the center temperature algebraically using a trial temperature profile of cubic order.

Comparisons of the three relevant temperatures have been conducted in a sphere because, among the regular bodies, the sphere is the configuration that exhibits the highest rate of cooling/heating because of its favorable volume/surface area ratio.

The validity of the theoretical study presented is affirmed by the close agreement of the approximate analytical predictions with a comprehensive base of exact analytical data.

Appendix: Two Fundamental Subproblems (Internal and External) That Constitute the Input for the Composite Lumped Model

First Fundamental Subproblem

The first subproblem is unsteady heat conduction in simple bodies with prescribed surface temperatures. Consider unsteady and unidirectional heat conduction in a regular solid body (long plate, long cylinder, and sphere) possessing uniform initial temperature T_i. Now, for $t > 0$, the body surface(s) is kept at a prescribed uniform temperature T_w. Accordingly, the mathematical formulation of this problem in dimensionless form is given by the one-dimensional heat conduction equation:

$$\frac{\partial \psi}{\partial \tau} = \frac{\partial^2 \psi}{\partial \eta^2} + \frac{c}{\eta}\frac{\partial \psi}{\partial \eta} \tag{A1}$$

together with the initial and boundary conditions

$$\psi = 1, \qquad \tau = 0 \tag{A2}$$

$$\frac{\partial \psi}{\partial \eta} = 0, \qquad \eta = 0 \tag{A3}$$

$$\psi = 0, \qquad \eta = 1 \tag{A4}$$

where the variables are defined by

$$\psi = \frac{T - T_w}{T_i - T_w}, \qquad \tau = \frac{t}{R^2/\alpha_s}, \qquad \eta = \frac{r}{R} \tag{A5}$$

Method of Separation of Variables

The exact temperature distributions $\psi(\eta, \tau)$ for each of the three configurations are taken from Arpaci.[1] They are described as follows.

Long plate:

$$\psi(\eta, \tau) = 2\sum_{n=0}^{\infty} \frac{(-1)^n}{\lambda_n R} \exp\left[-(\lambda_n R)^2 \tau\right] \cos[(\lambda_n R)\eta] \tag{A6}$$

where the eigenvalues are $\lambda_n R = (2n+1)\pi/2$, $n = 0, 1, 2, \ldots$.

Long cylinder:

$$\psi(\eta, \tau) = 2\sum_{n=1}^{\infty} \frac{\exp\left[-(\lambda_n R)^2 \tau\right] J_0[(\lambda_n R)\eta]}{(\lambda_n R) J_1(\lambda_n R)} \tag{A7}$$

where the eigenvalues $\lambda_n R$ are the positive roots of $J_0(\lambda_n R) = 0$.

Sphere:

$$\psi(\eta, \tau) = 2\sum_{n=0}^{\infty} (-1)^{n+1} \exp\left[-(\lambda_n R)^2 \tau\right] \frac{\sin[(\lambda_n R)\eta]}{(\lambda_n R)\eta} \tag{A8}$$

where the eigenvalues are $\lambda_n R = n\pi$, $n = 1, 2, 3, \ldots$.

Once the temperature distributions for each of the geometries have been determined, the generalized mean temperature for the three geometries can be expressed in dimensionless form as

$$\psi_m(\tau) = c\int_0^1 \psi\eta^{c-1}\,\mathrm{d}\eta \tag{A9}$$

where c is the geometric parameter.

Also, because the local internal Nusselt number Nu_s is a dimensionless representation of the local internal convective coefficient h_s, it can be obtained by

$$Nu_s = \frac{h_s(2R)}{k_s} = -\left[\frac{2(\partial\psi/\partial\eta)|_{\eta=1}}{\psi_m}\right] \tag{A10}$$

For the construction of the Nusselt number Nu_s, the ratio between the temporal variation of the temperature derivative at the surface in the numerator and the temporal variation of the mean temperature in the denominator needs to be obtained with great accuracy. The numerical evaluation of the quotient of two infinite series was done with the help of a symbolic algebra code Maple V (see Char et al.[16]).

Furthermore, the mean, internal Nusselt number $\overline{Nu}_s$ may be computed from its formal definition via the integral

$$\overline{Nu}_s = \frac{1}{\tau}\int_0^\tau Nu_s\,\mathrm{d}\tau \tag{A11}$$

or from the alternate form

$$\ell n\,\psi_m = (c/2)\overline{Nu}_s\tau \tag{A12}$$

Recall that the Nusselt number $\overline{Nu}_s$ is one of the two primary ingredients in the calculation of the mean, overall Nusselt number $\overline{Nu}_{ov}$, in Eq. (12). A regression analysis of the Nusselt number $\overline{Nu}_s$ vs τ data furnishes the following correlation equation:

$$\overline{Nu}_s^2 = \overline{Nu}_{s,\infty}^2 + (b/\tau) \tag{A13}$$

where the asymptotic Nusselt numbers for long times $t\to\infty$, $\overline{Nu}_{s,\infty}$, are computed with the first term in the respective infinite series for each body. The corresponding values of Nusselt number $\overline{Nu}_{s,\infty}$ are listed in Table A1. How good the three curve fits arc is reflected by high values of the correlation coefficients of the order of $R^2 \geq 0.9998$.

Inasmuch as the constant b is almost insensitive to the shape of the bodies (Table A1), an approximate mean value $b_{mean} = 5.1321$, may replace the specific values of b without incurring in appreciable errors.

TMOL for Short Times

The idea behind TMOL, also known as Rothe's method,[17] is to substitute the time derivative of the heat conduction equation (A1), by a two-point, backward finite difference formulation $[\psi^{(p+1)} - \psi^{(p)}]/\Delta\tau$. In this average derivative, the superscripts p and $(p+1)$ signify present and future time levels that are separated by a time step $\Delta\tau$. In principle, the aim of this operation is to break down the partial differential equation (A1) into a sequence of second-order ordinary differential equations [or two-point boundary-value problems (BVP)], which have the general structure

$$\frac{\mathrm{d}^2\psi^{(p)}}{\mathrm{d}\eta^2} + \frac{c}{\eta}\frac{\mathrm{d}\psi^{(p)}}{\mathrm{d}\eta} = \frac{\psi^{(p)} - \psi^{(p-1)}}{\Delta\tau}, \qquad p = 0, 1, \ldots, P \tag{A14}$$

Table A1 Constants $\overline{Nu}_{s,\infty}$ and b for Eq. (A13)

Body	$\overline{Nu}_s, \infty$	b
Long plate	$2(\pi/2)^2$	5.1253
Long cylinder	$(2.4048)^2$	5.1322
Sphere	$2(\pi^2/3)$	5.1387

For convenience, these BVP may be formed with equal time steps $\Delta\tau$. The initial condition of Eq. (A2) becomes $\psi^{(p-1)} = 1$ at $\tau = 0$. The boundary conditions come from Eqs. (A3) and (A4) and are rewritten, respectively, as

$$\frac{\mathrm{d}\psi^{(p)}}{\mathrm{d}\eta} = 0, \qquad \eta = 0 \tag{A15}$$

$$\psi^{(p)} = 0, \qquad \eta = 1 \tag{A16}$$

One time step $\Delta\tau$ (1-TMOL) is discussed next. The initial condition of Eq. (A2) is $\psi^{(0)} = 1$ at $\tau = 0$. Then, introducing $\psi^{(0)} = 1$ into Eq. (A14) furnishes the first BVP:

$$\frac{\mathrm{d}^2\psi^{(1)}}{\mathrm{d}\eta^2} + \frac{c}{\eta}\frac{\mathrm{d}\psi^{(1)}}{\mathrm{d}\eta} - \frac{\psi^{(1)}}{\tau} = -\frac{1}{\tau} \tag{A17}$$

where the boundary conditions are

$$\frac{\mathrm{d}\psi^{(1)}}{\mathrm{d}\eta} = 0, \qquad \eta = 0 \tag{A18}$$

$$\psi^{(1)} = 0, \qquad \eta = 1 \tag{A19}$$

For simplicity, the time step $\Delta\tau$ in Eq. (A17) has been replaced by τ and the superscripts are dropped. Now, by the specifying of the numerical values of c (= 1, 2, and 3) in Eq. (A17), the analytic solutions may be obtained immediately for the three coordinate systems.

For the long plate, the temperature distribution

$$\psi = 1 - \frac{\cosh(\eta/\sqrt{\tau})}{\cosh(1/\sqrt{\tau})} \tag{A20}$$

leads to the asymptotic mean, internal Nusselt number $\overline{Nu}_{s,0}$:

$$\overline{Nu}_{s,0} = -(2/\tau)\,\ell n[1 - \tanh(1/\sqrt{\tau})/\sqrt{\tau}] \tag{A21}$$

For the long cylinder, the temperature distribution

$$\psi = 1 - \frac{I_0(\eta/\sqrt{\tau})}{I_0(1/\sqrt{\tau})} \tag{A22}$$

leads to the asymptotic mean, internal Nusselt number $\overline{Nu}_{s,0}$:

$$\overline{Nu}_{s,0} = -\frac{1}{\tau}\left[1 - \frac{\sqrt{\tau}I_1(1/\sqrt{\tau})}{I_0(1/\sqrt{\tau})}\right] \tag{A23}$$

For the sphere, the temperature distribution

$$\psi = 1 - \frac{1}{\eta}\frac{\sinh(\eta/\sqrt{\tau})}{\sinh(1/\sqrt{\tau})} \tag{A24}$$

leads to the asymptotic mean, internal Nusselt number $\overline{Nu}_{s,0}$:

$$\overline{Nu}_{s,0} = -\frac{2}{3\tau}\,\ell n\left\{1 - \frac{3\tau[(1/\sqrt{\tau})\cosh(1/\sqrt{\tau}) - \sinh(1/\sqrt{\tau})]}{\sinh(1/\sqrt{\tau})}\right\} \tag{A25}$$

Of course, certain precautions need to be taken into account before using the preceding Nusselt number $\overline{Nu}_{s,0}$ equations, principally due to the nature of the two-point, backward finite difference formulation embedded into them. As expected, the practical use of the three evaluated-in-time Eqs. (A21), (A23), and (A25) are limited to short times, that is, $\tau \to 0$. The reason for this confinement is because the backward finite difference formulation is only first-order accurate[17] and, consequently, its error is also of order $\Delta\tau$.

The separate expressions for Nusselt numbers $\overline{Nu}_{s,0}$ and $\overline{Nu}_{s,\infty}$ are susceptible to time, the former is valid for short times, whereas the latter is valid for large times. With the aim at predicting Nusselt number $\overline{Nu}_s$ at all times, both equations for $\overline{Nu}_{s,0}$ and $\overline{Nu}_{s,\infty}$ may be

encapsulated into a blending correlation equation (see Churchill and Usagi[18]). Thus, the end product is expressed in compressed form by

$$\overline{Nu}_s = \left(\overline{Nu}^n_{s,0} + \overline{Nu}^n_{s,\infty}\right)^{1/n} \tag{A26}$$

where the adjusting parameter seems to be $n = 2$.

Semi-Infinite Region for Short Times

The mathematical formulation of this problem is given by the one-dimensional heat conduction equation

$$\frac{\partial \psi}{\partial \tau} = \frac{\partial^2 \psi}{\partial \eta^{*2}} + \frac{c}{\eta^*}\frac{\partial \psi}{\partial \eta^*} \tag{A27}$$

and the initial and boundary conditions

$$\psi = 1, \qquad \tau = 0 \tag{A28}$$

$$\psi = 0, \qquad \eta^* = 0 \tag{A29}$$

$$\lim \psi = 0, \qquad \eta^* \to \infty \tag{A30}$$

The resulting instantaneous surface heat fluxes q_w for the three configurations may be taken from Carslaw and Jaeger.[19] From here, the time-average surface heat fluxes may be calculated and channeled thorough the asymptotic mean, internal Nusselt number $\overline{Nu}_{s,0}$. Accordingly, the generalized formula for the three shapes is given by

$$\overline{Nu}_{s,0} = c + (4/\sqrt{\pi\tau}) \tag{A31}$$

which is valid for Fourier numbers τ less than 0.05 for the long plate, 0.04 for the long cylinder, and 0.03 for the sphere, respectively.[13] Likewise, predictions of the Nusselt number $\overline{Nu}_s$ may be obtained by the same blending correlation equation (A26).

As far as the time domain is concerned, the semi-infinite region approach is more restrictive than the 1-TMOL, because the latter applies to much larger times.

Second Fundamental Subproblem

The second subproblem is steady heat convection between the isothermal regular bodies and a fluid. The other primary ingredient that is vital in Eq. (12) is the Biot number Bi. We should keep in mind that Eq. (11) establishes the relationship between Biot number Bi and the mean external Nusselt number $\overline{Nu}_f$. Numerical values of Nusslet Number $\overline{Nu}_f$ usually emanate from theoretical and/or empirical correlation equations for laminar/turbulent forced convection past long plates, long cylinders, and spheres. These correlation equations are traditionally reported in textbooks on heat transfer (see Kreith and Bohn[20]) and do not need to be repeated here.

Acknowledgments

The author appreciates the suggestion given by Juan C. Morales, the University of Texas at Austin, during the course of the calculations.

References

[1]Arpaci, V., *Conduction Heat Transfer*, Addison–Wesley, Reading, MA, 1966.

[2]Grigull, U., Bach, J., and Sanders, H., "Näherungslösungen der Nichtstationaren Wärmeleitung," *Forschung im Ingenieurwesen*, Vol. 32, 1966, pp. 11–18.

[3]Grigull, U., and Sandner, H., *Heat Conduction*, Hemisphere, Washington, DC, 1984.

[4]Gurney, H. P., and Lurie, J., "Charts for Estimating Temperature Distributions in Heating and Cooling of Solid Shapes," *Industrial Engineering Chemistry*, Vol. 15, 1923, pp. 1170–1172.

[5]Boelter, L. M. K., Cherry, V. H., Johnson, H. A., and Martinelli, R. C., *Heat Transfer Notes*, Univ. of California Publ., Berkeley, CA, 1945; also McGraw–Hill, New York, 1965.

[6]Heisler, M. P., "Temperature Charts for Induction and Constant Temperature Heating," *Transactions of the American Society of Mechanical Engineers*, Vol. 69, 1947, pp. 227–236.

[7]Gebhart, B., *Heat Conduction and Mass Diffusion*, McGraw–Hill, New York, 1993.

[8]Gröber, H., *Einführung in die Lehre von der Wärmeübertragung*, Springer, Berlin, 1926.

[9]Gröber, H., Erk, S., and Grigull, U., *Fundamentals of Heat Transfer*, McGraw–Hill, New York, 1961.

[10]Stevens, J. W., and Luck, R., "Explicit Approximations for All Eigenvalues of the 1-D Transient Heat Conduction Equations," *Heat Transfer Engineering*, Vol. 20, 1999, pp. 35–41.

[11]Adebiyi, G. A., "A Single Expression for the Solution of the One-Dimensional Transient Conduction Equation for the Simple Regular Shaped-Bodies," *Journal Solar Energy Engineering*, Vol. 117, 1995, pp. 158–160.

[12]Ribando, R. J., and O'Leary, G. W., "Teaching Module for One-Dimensional, Transient Conduction," *Computer Applications in Engineering Education*, Vol. 6, 1998, pp. 41–51.

[13]Luikov, A. V., *Analytical Heat Diffusion Theory*, Academic, New York, 1968.

[14]Goodman, T. R., "Application of the Integral Method to Transient Non-Linear Heat Transfer," *Advances in Heat Transfer*, edited by T. F. Irvine Jr., and J. P. Hartnett, Vol. 1, Academic, New York, 1964, pp. 51–122.

[15]Langston, L. S., "Heat Transfer from Multidimensional Objects Using One-Dimensional Solutions for Heat Loss," *International Journal of Heat and Mass Transfer*, Vol. 25, 1982, pp. 149, 150.

[16]Char, B. W. et al., *Maple V Library Reference Manual*, Springer-Verlag, New York, 1991.

[17]Rothe, E., "Zweidimensionale Parabolische Randwertaufgaben als Grenzfall Eindimensionaler Randwertaufgaben," *Mathematishe Annalen*, Vol. 102, 1930, pp. 650–670.

[18]Churchill, S. W., and Usagi, R., "A General Expression for the Correlation of Rates of Transfer and Other Phenomena," *AIChE Journal*, Vol. 18, 1972, pp. 1121–1128.

[19]Carslaw, H. S., and Jaeger, J. C., *Conduction of Heat in Solids*, 2nd ed., Oxford Univ. Press, London, 1959.

[20]Kreith, F., and Bohn, M. S., *Principles of Heat Transfer*, 5th ed., West, New York, 1993.